A New Model for Neutron Reflectometry of Adsorbed Surfactant Aggregates

Jamie C. Schulz and Gregory G. Warr*

School of Chemistry, University of Sydney, Sydney NSW 2006, Australia

William A. Hamilton

Solid State Division, Oak Ridge National Laboratory, Oak Ridge, Tennessee 37831-6393

Paul D. Butler

NIST Center for Neutron Research, National Institute of Standards and Technology, 100 Bureau Drive, Gaithersburg, Maryland 20899-8562

Received: March 9, 1999

A new interpretation of neutron reflectivity data for surfactants adsorbed on hydrophilic solid surfaces has been developed. Motivated by recent atomic force microscopy results, a model of the adsorbed layer is constructed based upon an adsorbed layer consisting of discrete, micelle-like surfactant aggregates of well-defined geometries. Scattering length density profiles and reflectivity curves are calculated for conventional, laterally unstructured adsorbed layers (a bilayer), as well as for cylindrical and spherical surfactant aggregates adsorbed on a hydrophilic surface. It is shown that treating such structured surfactant films as bilayers often results in a good fit to neutron reflectivity data, but that fit parameters lead one to underestimate the film thickness and overestimate the fractional surface coverage by the adsorbed film.

Introduction

Surfactant adsorption onto hydrophilic solid surfaces is an important phenomenon in many industrial and chemical processes. Traditionally, surfactant adsorption has been characterized by adsorption isotherms,[1] which show the amount of surfactant adsorbed onto the hydrophilic solid surface and give an insight into the adsorption mechanism. Other experimental methods employed to elucidate adsorption mechanisms include the surface force apparatus,[2−7] ellipsometry,[8−13] fluorescence quenching,[14−18] small angle neutron scattering,[19−22] and NMR.[23−29]

Neutron reflectometry has emerged over the past decade as an important tool for interpreting the structure of adsorbed surfactant films.[30−35] The primary interpretation of the adsorbed surfactant film has been a bilayer-type film consisting of three distinct regions: a surfactant headgroup region closest to the hydrophilic solid surface, a tail region, and finally another headgroup region adjacent to the bulk solution. Other, more complex, variations on the bilayer model have been considered, e.g., in which the interfacial headgroup region is compressed and hence is thinner than the bulk solution headgroup region.[31,36] The coverage of the surfactant film is rarely found to be unity, and this has been interpreted as being a "defect bilayer-type" structure or "islands" of surfactant.[30−35]

However, the precise structure of the surfactant aggregates has remained unclear until recently when direct visualization of the adsorbed surfactant film was accomplished using non-contact atomic force microscopy (AFM).[37−41] These results have shown adsorbed surfactants to form well-defined, regular geometric structures at high surface coverage (above the critical micelle concentration) on hydrophilic surfaces such as mica and glass, and have been interpreted as adsorbed aggregates, or micelles. Bilayer, cylindrical, and spherical surfactant aggregate structures have all been observed in various adsorbed films on a range of hydrophilic surfaces, paralleling the known surfactant aggregate geometries in bulk phases.

In neutron reflectometry, as in most scattering experiments, structure cannot be directly obtained from experimental data. Rather, results are generally fitted by assuming a model which describes the structure of the interface, calculating the reflectivity curve, and comparing it with the experimental data. The parameters within the model of the interface are then systematically varied, usually by a least-squares fitting procedure until an adequate fit is obtained.

The problem inherent in this approach is the reliance upon the correctness of the initially assumed structure of the interface. As reflectivity is the square of the transform of the density profile normal to the interface, crucial information about the phase of the Fourier transform is lost. This may result in satisfactory fits to the experimental data being achieved even if the structure of the interface is wrong. This problem in reflectivity is known as the *Inverse Problem* and has been discussed in detail elsewhere.[42−44]

Similar phenomena may be observed in small angle neutron scattering, where an assumed micelle shape determines the fitted structure factor. Two plausible geometries can fit $I(Q)$ equally well, but with substantially different interpretations.[45,46]

In this paper we address the implications of the recent AFM observations with relation to the structure of the adsorbed films in the interpretation of neutron reflectivity data, particularly for surfactants adsorbed from solution onto solid, hydrophilic surfaces.[47] Specifically, we ask how our interpretation of neutron reflectometry is affected if the adsorbed layer is indeed made up of discrete spherical or cylindrical micelles, but fitted

* Corresponding author e-mail: g.warr@chem.usyd.edu.au.

10.1021/jp990827j CCC: $18.00
Published on Web 11/24/1999

assuming a bilayer or partial bilayer. The scattering profile from each geometry is calculated and compared, and the effect of contrast variation within the bulk solution examined.

Calculation of Reflectivity Curves for Aggregated Structures. In this section we describe the method by which neutron reflectivity curves are generated for different adsorbed surfactant aggregate structures at the solid/solution interface.

Experimental Considerations. The experimental system modeled here is based on (fully hydrogenated) surfactant at high surface coverage adsorbed onto crystalline quartz, in equilibrium with its own bulk solution in either D_2O or a mixture of D_2O and H_2O. All components within the simulations will be based upon the parameters used for this system. Commonly used surfaces in neutron reflectometry include quartz,[32,33,47] silica,[30,31,35] and oxidized silicon.[31,34] Our choice of a homogeneous solid superstrate is made to reduce complications in interpretation of the simulations with, e.g., an oxidized SiO_2 layer on silicon.[31,34]

In these simulations we assume for simplicity that the surfactant film consists of aggregates which are evenly distributed over the solid surface. The effect of uneven distribution or patchy surface coverage is discussed further below. We note that there has been no visual evidence of segregation of surfactant aggregates observed at high coverage in AFM studies of adsorbed surfactant films.

Experimentally neutron reflectometry of adsorbed surfactant films is limited to a small scattering vector range due to (i) the weak reflectivity signal arising from the thin (~50 Å) film and (ii) the low contrast due to the fact that the surface coverage is less than unity. Reflectivities less than 10^{-6} are thus not usually experimentally achievable as background noise from the solution is of this order of magnitude. Curves reported here are thus fitted over the reflectivity range $10^0 - 10^{-6}$ for cylinders and spheres.

The surfactant−solvent−solid system consists of a perfectly smooth, homogeneous, solid superstrate with a scattering length density $\beta_{\text{superstrate}} = 4.16 \times 10^{-6}\text{Å}^{-2}$,[48] surfactant molecules of alkyl hydrocarbon composition with length $l = 25$ Å and scattering length density $\beta_{\text{surfactant}} = -0.5 \times 10^{-6}\text{Å}^{-2}$,[49] and a bulk solution of scattering length density $\beta_{\text{bulk}} = 6.36 \times 10^{-6}\text{Å}^{-2}$,[48] for pure D_2O. The surfactant molecules are considered to be of homogeneous alkyl hydrocarbon composition, i.e., no segregation between headgroup and tail, to reduce the complexity of the system in this case. Also, we neglect any change in scattering length density of the bulk solution due to dissolved solute.

In some systems the H/D ratio for the bulk solution has been chosen so that the scattering length density is matched to that of the solid superstrate. This condition is referred to as "contrast-matching".

Interface Construction and Reflectivity Calculation. In specular reflectivity experiments at the solid/liquid interface, the incident neutron beam enters the solid superstrate and strikes a flat surface at angle θ, which is in contact with the solution. The intensity of the reflected beam is recorded as a function of the scattering vector, Q, which is perpendicular to the interface, where $Q = 4\pi \sin\theta/\lambda$ and λ is the wavelength of the radiation. The reflection of a beam of neutrons is directly related to the composition and structure normal to the interface, which is described by the scattering length density profile given by

$$\beta(z) = \sum_i b_i n_i(z) \tag{1}$$

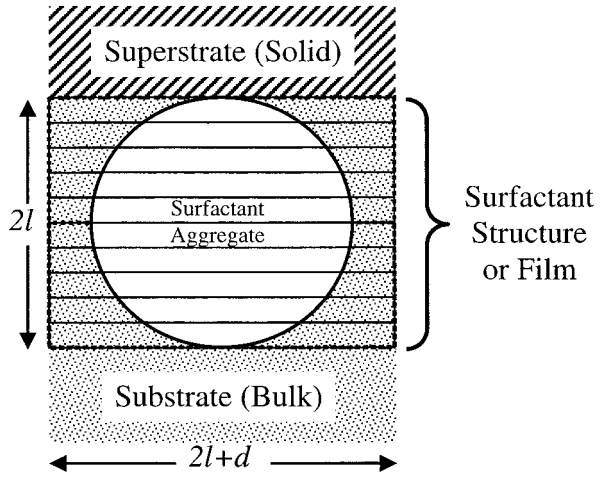

Figure 1. Diagram of the unit cell for a cylinder used to calculate the scattering length density profile. The interface is divided into n layers: $n = 40$ in the calculations, here $n = 10$ layers in this figure, with an overall thickness equal to twice the length of the surfactant molecule. Coverage is altered by adjustment of the separation between structures, d, giving overall dimensions for the unit cell of $2l \times (2l + d)$.

where b_i is the bound coherent scattering length of nucleus i and $n_i(z)$ is its number density profile normal to the interface.

The specular reflection coefficient for neutrons is an optical transform in the scattering vector, Q, of the scattering length density profile. At high Q and low reflectivities, this transform is given by the Rayleigh approximation[50,51]

$$R(Q) \approx \frac{(4\pi)^2}{Q^4} \left| \int_{-\infty}^{\infty} \frac{d\beta}{dz} e^{-iQz} dz \right|^2 \tag{2}$$

where $d\beta/dz$ is the gradient of the scattering length density as a function of depth in the sample.

The analysis of reflectivity data as discussed earlier usually proceeds by comparison of experimental data with models calculated assuming that the interfacial structure, $\beta(z)$, can be replaced by a series of discrete homogeneous layers. The reflectivity is then calculated using an exact layer-by-layer method.[52]

For a bilayer-type structure with coverage less than unity, a fractional coverage, θ, is often invoked as a fitting parameter for the bilayer.[30−35] The scattering length density, β, of the layer is then just the weighted average for a "wet" layer

$$\beta = \theta\beta_{\text{surfactant}} + (1 - \theta)\beta_{\text{bulk}} \tag{3}$$

where $\beta_{\text{surfactant}}$ and β_{bulk} are the scattering length densities of the surfactant and the bulk solution, respectively.

To calculate the reflectivity curve we consider a single surfactant aggregate within a unit cell, which is representative of the adsorbed film (see Figure 1). The thickness of the adsorbed film for all three structures is twice the length of a surfactant molecule, $2l$. The unit cell is divided into n layers normal to the interface; the scattering length density of any layer is then the weighted average scattering length density contribution of the surfactant aggregate and the bulk solution. (Although the reflectivity from homogeneous spheres and cylinders could be calculated without discretizing the data, we prefer to do so as this allows later generalization of our method to include surfactant headgroups (core−shell aggregates) and other, more complex structures.) The number of layers, n, used to divide the interface in the calculation is 40 in this study. For a film 50 Å thick, each layer is thus 1.25 Å thick. In Figure 1, we show

a cross-section of a cylinder as a representative example of the interface construction.

Fractional coverage is obtained from eq 3 using the best-fit scattering length density of a "wet" bilayer-type structure. For cylindrical and spherical structures fractional coverage is a unique function of separation between aggregates, d (see below).

Once the scattering length density profile perpendicular to the surface is determined, the total reflectivity from the multilayer interface is then calculated using an exact layer-by-layer method.[52]

Cylindrical Aggregates. An adsorbed cylinder is represented by a circular cross-section enclosed within a rectangle, illustrated in Figure 1. The dimensions of the rectangle are $2l \times (2l + d)$, where d is the separation between the cylinders. The fractional coverage of the surfactant can be determined from the ratio of the cross-sectional area of the cylinder to the area of the rectangle. A change in separation, d, determines the fractional coverage

$$\theta_{\text{cylinder}} = \frac{\pi l}{2(2l + d)} \tag{4}$$

The maximum fractional coverage occurs when the cylinders are in contact ($d = 0$), thus $0 < \theta < \pi/4 \approx 0.79$.

Spherical Aggregates. The unit cell of an adsorbed spherical aggregate is a sphere enclosed within a hexagonal box. As before, the box has a thickness equal to twice the length of the surfactant molecule, and the distance between the parallel sides is $2l + d$. The fractional coverage of the adsorbed layer in this case is

$$\theta_{\text{sphere}} = \frac{\pi l^2}{3\sqrt{3}(l + d/2)^2} \tag{6}$$

For spheres in a hexagonal lattice, $0 < \theta < \pi l 3\sqrt{3} \approx 0.60$.

It should be noted that the scattering length density profile, and hence reflectivity, is not sensitive to the lateral arrangement of these aggregates. A square lattice yields a different $\theta(d)$, but $R(Q, \theta)$ is unchanged. Likewise, cylinder orientation and, to first order, flexibility does not affect θ or (specular) reflectivity.

While the packing of surfactant aggregates does not have an effect upon reflectivity, the macroarrangement of such aggregates into separate domains on the solid surface ($\approx 10^4$ Å), which are greater than the experimental neutron coherence length, would have an effect. In this case the overall reflectivity would be the weighted average of the reflectivities of the clean and aggregate-coated interfaces. Large-scale separation of the adsorbed layer into domains has been considered previously, but was determined to be negligible.[30,33]

A computer program, ReflectJCS,[54] is used to generate scattering length density profiles and calculate the corresponding reflectivity curves. Input fitting parameters are the length of the surfactant molecules and coverage of the surfactant film.

Results

Complete Bilayer. Figure 2 shows typical neutron reflectivity curves $R(Q)$ for a clean, sharp interface and a homogeneous thin (50 Å) film on a solid superstrate under the two bulk solvent contrast conditions: D_2O and solvent contrast-matched to superstrate. Data are shown as logarithm of the reflectivity against the scattering vector, Q. The inset shows the scattering length density profiles, $\beta(z)$, corresponding to each $R(Q)$.

The reflectivity for a clean interface (dashed line) shows a total reflection plateau at low Q for a positive scattering length density change ($\beta_{\text{bulk}} - \beta_{\text{superstrate}}$) and the expected Q^{-4} dependence (eq 2) above the critical angle. There is no reflectivity from the clean interface with contrast-matched bulk solution: a reflectivity signal is observed only if an adsorbed layer is present.

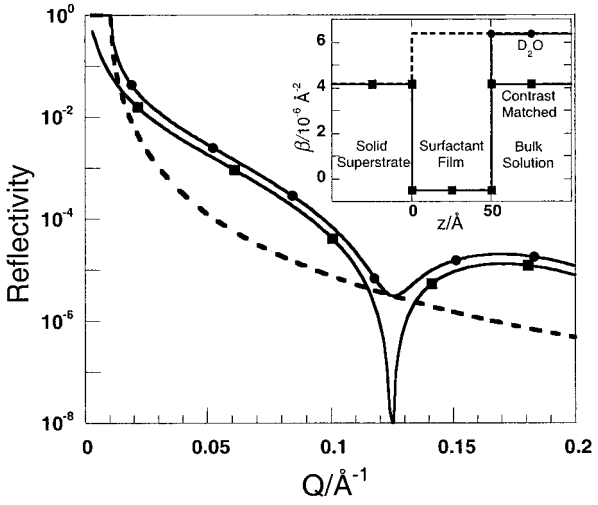

Figure 2. Reflectivity curves for the bilayer structure, at 100% coverage, against D_2O (●), and contrast-matched D_2O/H_2O (■). Thickness, $2l = 50$ Å, $\beta_{\text{surfactant}} = -0.5 \times 10^{-6}$Å^{-2}, $\beta_{\text{bulk}} = 6.36 \times 10^{-6}$ Å^{-2}. The dashed line shows reflectivity from the uncoated interface against D_2O. Inset: Scattering length density profiles, $\beta(z)$, for the three reflectivity curves.

For a homogeneous adsorbed film on a solid superstrate, the two bulk solution conditions result in different reflectivity curves. In D_2O the critical angle observed for the clean interface is preserved. However, under contrast-matching conditions there is no plateau. Interference fringe minima occur in both reflectivity curves.

The thickness of the film may be directly obtained from the spacing of the interference fringes. The period of the interference minima (Q_{min}) is approximately equal to $2\pi/\tau$, where τ is the film thickness.[53] The interference fringe in Figure 2 for the thin film using both bulk solution contrasts occurs at $Q_{\text{min}} = 0.125$ Å^{-1}, which corresponds to the film thickness of 50 Å.

Partial Bilayer. Reflectivity curves calculated for bilayers with surface coverages $0 < \theta < 1$ are shown in Figure 3 at the same two contrast conditions: D_2O and solvent contrast-matched to superstrate.

A change in fractional surface coverage, θ, has a significant effect on the observed reflectivity profile. Reflectivity decreases overall with decreasing θ due to the reduced contrast between the film, the solid superstrate, and the bulk solution. This is clearly seen in the scattering length density profiles, shown as insets.

As with the complete bilayer, an interference minimum is present for both contrast conditions at $Q = 0.125$ Å^{-1} for all surface coverages in contrast-matched solvent, and at surface coverages above $\theta = 0.32$ in D_2O, where the bilayer film and solid are contrast-matched.

Reflectivity falls below that of the clean interface for $\theta = 0.20$ with D_2O, and there are also two interference minima in the data. This is due to the change from a "trough" to a "step" in the scattering length density profile[55] (see inset, Figure 3a) and consequent change in phase of the reflected beam at $z = 0$.

Adsorbed Aggregates: Cylinders and Spheres. Due to the similarity between the scattering length density profiles and reflectivity curves for adsorbed cylinders and spheres, these will be considered together. The fractional surface coverage can vary

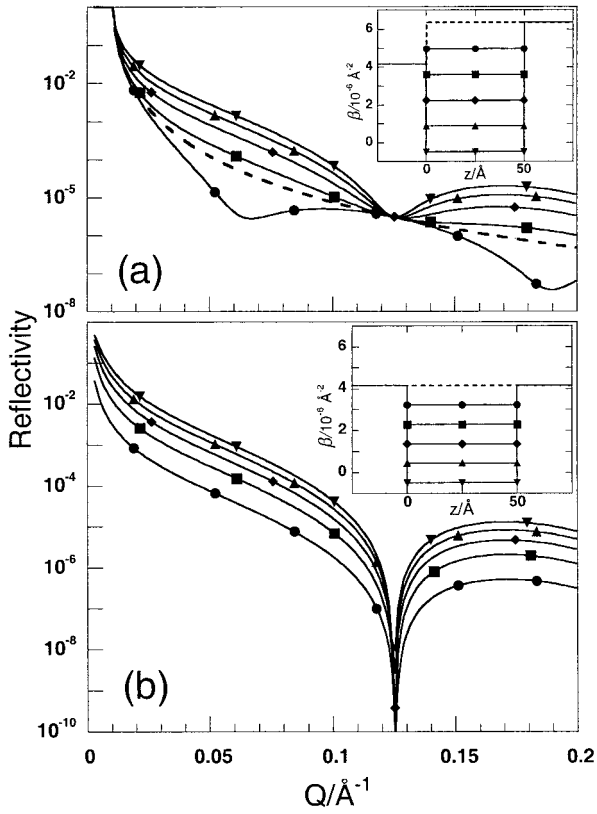

Figure 3. Reflectivity curves for the bilayer structure, at varying coverage, with (a) D_2O, $\beta_{bulk} = 6.36 \times 10^{-6}$ Å^{-2} and (b) contrast-matched water, $\beta_{bulk} = 4.16 \times 10^{-6}$Å^{-2} as the bulk solution. Thickness = 50 Å. $\theta = 0.0$ (- - -) and $\theta = 0.32$ in Figure 3a, 0.20 (●), 0.40 (■), 0.60 (◆), 0.80 (▲), 1.00 (▼). Inset: Scattering length density profile for the calculated reflectivity curves.

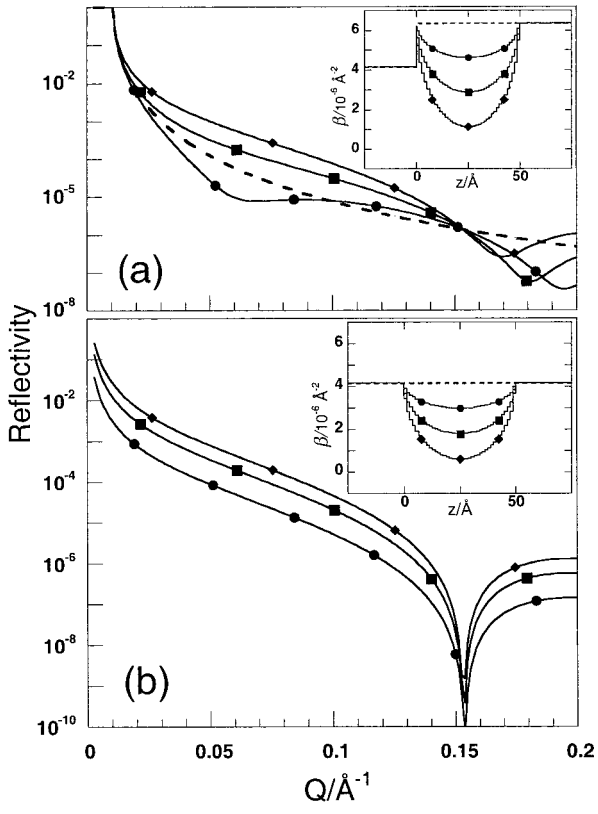

Figure 4. Reflectivity curves for the cylinder structure, at varying coverage, with (a) D_2O, $\beta_{bulk} = 6.36 \times 10^{-6}$ Å^{-2} and (b) contrast-matched water, $\beta_{bulk} = 4.16 \times 10^{-6}$ Å^{-2} as the bulk solution. Thickness = 50 Å. $\theta = 0.0$ (- - -), 0.20 (●), 0.40 (■), 0.60 (◆). Inset: Scattering length density profile for the calculated reflectivity curves.

from 0 to 0.79 for cylinders (eq 4), and from 0 to 0.60 (eq 5) for spheres on a hexagonal lattice (0.52 on a square lattice). This is independent of molecular length.

Reflectivity curves were generated for adsorbed cylindrical and spherical aggregates for $\theta = 0-0.60$, using the same two bulk contrasts as above. These are shown in Figures 4 and 5, respectively.

The scattering length density profiles of cylindrical and spherical aggregates are shown as insets in Figures 4 and 5. The profile of a spherical aggregate is deeper and narrower than a cylindrical aggregate at the same θ, but otherwise they are similar.

The reflectivity curves in contrast-matched solvent (Figures 4b and 5b) closely resemble the partial bilayer reflectivity curves (Figure 3b). A single interference minimum is observed at $Q_{min} = 0.154$ Å^{-1} for cylindrical aggregates and $Q_{min} = 0.173$ Å^{-1} for spherical aggregates at all fractional surface coverages. As before, reflected intensity increases with increasing surface coverage.

Reflectivity curves in D_2O show some departures from previously observed behavior. It is convenient to divide these curves into low Q ($Q < Q_{min}$) and high Q ($Q > Q_{min}$) regimes. All reflectivity curves coincide at $Q = Q_{min}$, where they also intersect the reflectivity curve of the clean interface.

The low Q behavior of these curves is similar to that seen for partial bilayers. The presence of an adsorbed layer increases reflectivity at low Q for surface coverages above 0.4, and reflected intensity increases with increasing fractional surface coverage, θ.

For $\theta = 0.2$, reflectivity from the adsorbed film drops below that of the bare interface. Again this can be broadly identified with a change from a "trough" to a "step" in the scattering length density profile (see insets to Figures 4a and 5a). However, for these structured aggregates the adsorbed film cannot be contrast-matched to the solid at all z.

The reflectivity of adsorbed spheres and cylinders in D_2O at high Q differs from the bilayer results markedly. Here the reflectivity falls below that of the clean interface for all θ, forming an interference minimum at a different Q from the contrast-matched solvent case. This interference fringe moves to larger Q as θ decreases.

Fitting a Bilayer Model to Reflectivity Curves. In Figure 6 neutron reflectivity curves are compared for the three different structures: bilayer, cylinders, and spheres at constant fractional film coverage of 0.50 and film thickness of 50 Å. The period of the interference fringes for the three structures increases in the order bilayer < cylinder < sphere. Neglecting refraction effects we have the approximate result that $\tau = 2\pi/Q_{min}$,[53] which gives the expected film thickness of 50 Å for the bilayer. Applying this approximation to contrast-matched reflectivity curves (Figure 6b) yields apparent film thicknesses of 40 Å for cylinders and 36 Å for spheres.

If we assume, as is common, that the reflectivity curves generated for cylindrical and spherical aggregates represent a laterally unstructured film and fit them accordingly, then an effective film thickness and coverage θ may be extracted. In the fitting procedure, the scattering length density of the surfactant film, solid and solvent are known, and the thickness and θ of the bilayer are optimized to obtain adequate fits to the reflectivity curves over the range $10^{-6} < R < 10^{0}$. For all of the fits described, the best fit parameter χ^2 is minimized.

Optimized best fits of the bilayer structure to adsorbed cylinder and sphere reflectivity curves are also shown in Figure

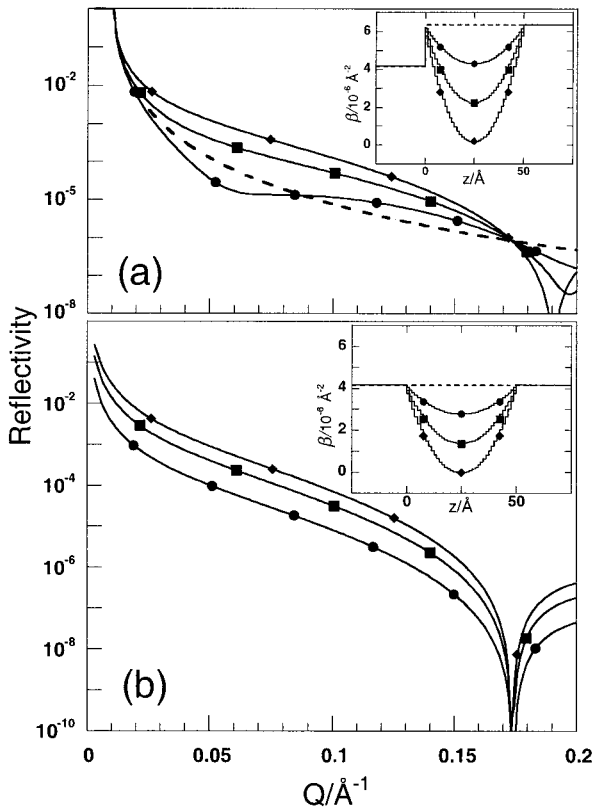

Figure 5. Reflectivity curves for the sphere structure, at varying coverage, with (a) D_2O, $\beta_{bulk} = 6.36 \times 10^{-6}$ Å^{-2} and (b) contrast-matched water, $\beta_{bulk} = 4.16 \times 10^{-6}$ Å^{-2} as the bulk solution. Thickness = 50 Å. $\theta = 0.0$ (- - -), 0.20 (●), 0.40 (■), 0.60 (◆). Inset: Scattering length density profile for the calculated reflectivity curves.

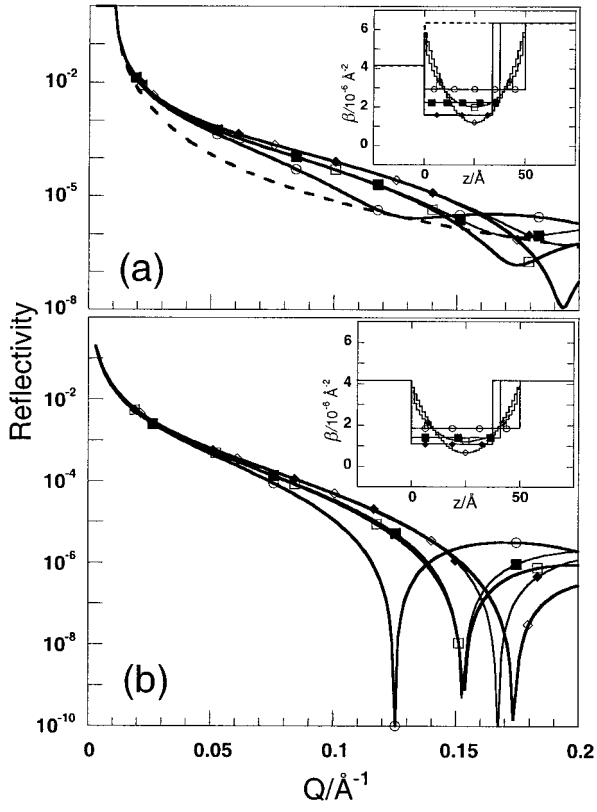

Figure 6. Reflectivity curves for 50 Å structured films at $\theta = 0.50$ for the three structures: bilayer, cylinder, and sphere, with (a) D_2O, $\beta_{bulk} = 6.36 \times 10^{-6}$ Å^{-2} and (b) contrast-matched water, $\beta_{bulk} = 4.16 \times 10^{-6}$Å^{-2} as the bulk solution. Inset: Scattering length density profile for the calculated reflectivity curves. Simulated curves: bilayer (○), cylinder (□), sphere (◇). Bilayer fit to cylinder (■) and sphere (◆). Here, - - - denotes bare (D_2O) interface.

6. The goodness of fit over the experimentally accessible R range is seen more clearly in Figure 7, where reflectivity is plotted as $R(Q) \times Q^4$ versus Q. The best-fit thickness and fractional coverage for all structures in both solvent contrasts are listed in Table 1.

Necessarily only the fit of the bilayer is perfect and gives the correct thickness and coverage. The bilayer fits of cylinders and spheres in both solvent contrasts yield surface coverages and apparent thicknesses which agree well with each other. However the fitted values differ markedly from our input values.

From a bilayer fit we would infer that the thickness of the adsorbed film decreases in the order bilayer > cylinder > sphere. The values obtained agree well with the thicknesses estimated above from the location of the interference minima. The differences between reflectivity curves are more pronounced at high Q, however the low reflectivities require greater experimental sophistication than is possible for all systems.

A bilayer fit to adsorbed aggregates also suggests that the *apparent* θ increases in the order bilayer < cylinder < sphere. These trends are the same for both solution contrasts studied. Overall there is little in the fitted reflectivity profiles to indicate that the simulated curves are not patchy bilayers of somewhat reduced thickness.

Discussion

Lu and Thomas[53] recently pointed out that $\theta = 1.0$ is rarely observed in neutron reflectometry, and patchy coverage is the usual explanation. The most significant feature of adsorbed films of structured aggregates such as cylinders and spheres is that they cannot produce 100% surface coverage. This is a natural consequence of the model, whereas a patchy bilayer is an ad hoc correction to a surface structure which should have $\theta = 1.0$. Fractional surface coverages reported in the literature derived from many techniques including atomic force microscopy,[37−41] ellipsometry,[8−13] fluorescence quenching,[14−18] and adsorption studies[57−61] are consistent with the maximum surface coverages expected for adsorbed spheres and cylinders. In particular, AFM images of double-chained surfactants adsorbed on mica, which do form bilayers, are not patchy on any of the length scales examined.[38]

In Table 2 the best-fit parameters of a patchy bilayer fit to the reflectivity data for cylinders and spheres at varying coverage with D_2O as the bulk solvent are listed. The bilayer-fitted coverages are always greater than the actual coverage, by about 20% for cylinders and 40% for spheres. Spheres close-pack ($d = 0$) at $\theta = 0.60$, but a bilayer fit to such a film gives an apparent 0.82 fractional coverage. Likewise, cylinders are close-packed at $\theta = 0.79$, whereas a bilayer fit gives $\theta = 0.93$. It may therefore be possible to discriminate at least between a patchy bilayer and structured aggregates by comparing surface coverages from sphere, cylinder, and bilayer fits to an experimental reflectometry curve, and by discarding any which are not physically realistic (i.e., $\theta_{spheres} > 0.60$, $\theta_{cylinders} > 0.79$, or $\theta_{bilayer} > 1$).

In experimental neutron reflectometry studies of adsorbed surfactant films it is common to carry out experiments with a variety of isotopically substituted adsorbing species in addition to varying solution contrast, thus providing a range of different scattering length density profiles, all arising from the same film structure. Coupled fits of such data sets are often advocated.

Selective deuteration of the adsorbed film (e.g., deuteration

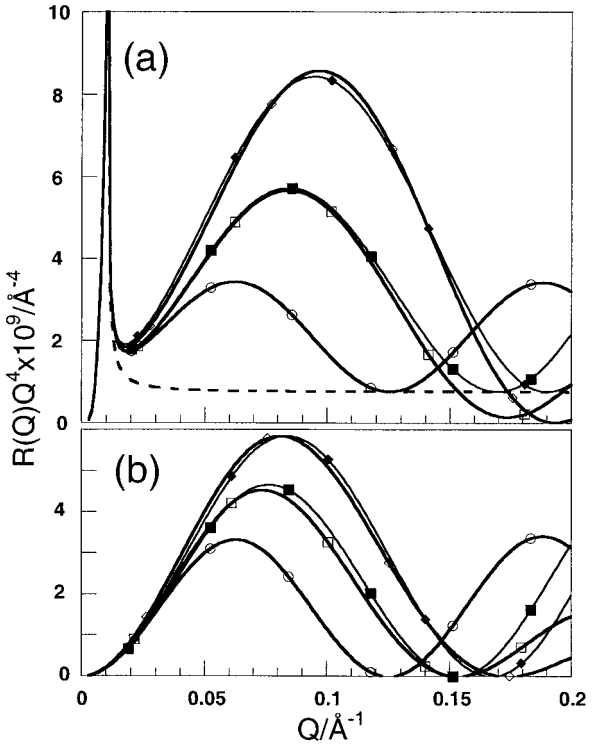

Figure 7. $R(Q) \times Q^4$ versus Q for 50 Å structured films at $\theta = 0.50$ for the 3 structures: bilayer, cylinder and sphere, with (a) D_2O and (b) contrast-matched water as the bulk solution. See Figure 6 insets for the corresponding scattering length density profiles. Simulated curves: bilayer (○), cylinder (□), sphere (◇). Bilayer fit to cylinder (■) and sphere (◆). Here, - - - denotes bare (D_2O) interface.

TABLE 1: Optimized Bilayer Fit Parameters for $\theta = 0.50$ Fractional Coverage Films of 50 Å Thick Bilayer, Cylinder, and Sphere Structures in D_2O and Contrast-Matched Solvent

	D_2O		contrast-matched solvent	
	fitted fractional coverage, θ	fitted thickness, τ/Å	fitted fractional coverage, θ	fitted thickness, τ/Å
bilayer	0.50	50	0.50	50
cylinder	0.59	38	0.59	42
sphere	0.69	34	0.67	38

TABLE 2: Bilayer Fit Parameters θ and τ for 50 Å Thick Cylinder and Sphere Structures in D_2O, Varying Fractional Coverage

actual coverage		0.10	0.20	0.30	0.40	0.50	0.60	0.70	0.79
bilayer fit to cylinders	τ/Å	48	50	30	37	38	39	40	40
	θ	0.11	0.23	0.37	0.48	0.59	0.71	0.83	0.93
bilayer fit to spheres	τ/Å	48	50	28	32	34	34	−	−
	θ	0.12	0.25	0.43	0.56	0.69	0.82	−	−

of part of the surfactant tails) has been used as evidence to support the bilayer structures for adsorbed films.[56] In this interpretation the film is subdivided into layers consisting primarily of H or D. In spherical or cylindrical micelles, however, a more complex model of the alkyl chain conformations and their distributions is required.[62−64]

In this model data we find little difference between the best-fit parameters derived from very different *solution* contrasts and little to suggest that coupled fitting would be advantageous. While the differences between fitted parameters obtained for films in D_2O and contrast-matched solvent are small and at the limit of experimental resolution, bulk solvent contrast variation studies do reveal a systematic trend providing another signature for distinguishing structured adsorbed films from bilayers.[35]

While interference minima of spheres and cylinders remain constant with decreasing surface coverage for contrast-matched conditions (Figures 4b and 5b), with D_2O as solvent they shift to larger Q (Figures 4a and 5a). This suggests a decrease in the apparent film thickness with decreasing fractional surface coverage. The fitted film thickness for fractional coverages less than 0.20 are close to the actual film thickness, whereas fractional coverages greater than 0.20 give the same result as the first order interpretation of increasing film thickness with increasing fractional surface coverage (see Table 2).

In principle a systematic study of adsorbed layers monitoring fringe position at varying surface coverages could therefore expose distinctions between different aggregate structures. Simply measuring reflectivity as a function of concentration (tracing an adsorption isotherm) may involve changes in both τ and θ (and possibly aggregate shape) with surface coverage, and so would not be particularly informative. However, the interaggregate spacing and hence surface coverage might be systematically varied for ionic surfactants by changing electrolyte concentration, counterion,[41] or pH,[38] as long as care was taken not to induce a shape change.

Limitations of the model. In this study we have used infinitely sharp interfaces between layers in our modeling. For real systems the solid superstrate is rough, and this will affect the reflectivity profile. The common approach to dealing with roughness in a laterally unstructured film is to convolute $\beta(z)$ with a Gaussian roughness of thickness σ.[50,51] A single roughness may be propagated through all layers, or each interface fitted separately. A specific geometrical model such as the present requires a specific model for roughness, which will be sensitive to details of aggregate shape at the surfactant/solid interface.

We have considered the surfactant molecules to be of homogeneous scattering length density in this study, neglecting the different scattering length densities of the hydrophilic head and hydrophobic tail. This problem, however, together with the case of core−shell structures such as nonionic micelles, poses no particular difficulty for our approach. Adsorbed films of partially deuterated molecules may be also dealt with in a like manner.

We have not included any deformation of the surfactant aggregates at the contact plane, which may occur upon adsorption. The general effect would be a smearing of the structural detail of $\beta(z)$, principally around $z = 0$ (see insets to Figures 4−7), and are not apparent over the Q range studied. Reducing the number of layers in our simulation achieves a coarse graining effect which blurs some structural detail on this length scale. The calculated reflectivity curves with n as low as eight layers (of thickness 6.25 Å) show no differences over the Q range reported.

Conclusions

We have developed a new approach by which to model neutron reflectivity data of adsorbed surfactant films based on the existence of discrete surfactant aggregates of well-defined geometry, consistent with recent AFM observations. Reflectivity curves from a laterally unstructured (patchy) bilayer, together with cylindrical and spherical surfactant aggregates, were modeled adsorbed onto a hydrophilic surface using a multilayer approach to describe the scattering length density profile.

It was shown that treating such structured surfactant films as bilayers underestimates the film thickness and overestimates the fractional surface coverage by the adsorbed film. However, solvent contrast variation yields self-consistent fitted parameters, and there are few clues that the fitted structure is wrong.

Our conclusions are cautionary. Mounting evidence for laterally structured surfactant films cannot be ignored in interpreting neutron reflectometry data. Assumption of, and fitting to, a laterally unstructured film may lead to underestimation of layer thickness and overestimation of surface coverage.

Acknowledgment. This work was funded by the Australian Research Council and the Australian Nuclear Science and Technology Organization. Oak Ridge National Laboratory is managed by Lockheed Martin Energy Research Corporation under contract DE-AC05-96OR22464 with the U.S. Department of Energy. J.C.S. acknowledges receipt of a Henry Bertie and Florence Mabel Gritton Postgraduate Scholarship from the University of Sydney.

References and Notes

(1) Bijsterbosch, B. H. *J. Colloid Interface Sci.* **1973**, *47*, 186−198.
(2) Kekicheff, P.; Christenson, H. K.; Ninham, B. W. *Colloids Surf.* **1989**, *40*, 31−41.
(3) Luckham, P. F.; Klein, J. *J. Colloid Interface Sci.* **1987**, *117*, 149−158.
(4) Pashley, R. M.; McGuiggan, P. M.; Horn, R. G.; Ninham, B. W. *J. Colloid Interface Sci.* **1988**, *126*, 569−578.
(5) Rutland, M. W.; Parker, J. L. *Langmuir* **1994**, *10*, 1110−1121.
(6) Rutland, M. W. *Colloids Surf. A* **1994**, *83*, 121−128.
(7) Xu, Z. H.; Ducker, W.; Israelachvili, J. *Langmuir* **1996**, *12*, 2263−2270.
(8) Tiberg, F. *J. Chem. Soc., Faraday Trans.* **1996**, *92*, 531−538.
(9) Tiberg, F.; Joensson, B.; Tang, J.-A.; Lindman, B. *Langmuir* **1994**, *10*, 2294−2300.
(10) Tiberg, F.; Joensson, B.; Lindman, B. *Langmuir* **1994**, *10*, 3714−3722.
(11) Luciani, L.; Denoyel, R. *J. Colloid Interface Sci.* **1997**, *188*, 75−80.
(12) Harwigsson, I.; Tiberg, F.; Chevalier, Y. *J. Colloid Interface Sci.* **1996**, *183*, 380−387.
(13) Brinck, J.; Tiberg, F. *Langmuir* **1996**, *12*, 5042−5047.
(14) Somasundaran, P.; Krishnakumar, S. *Colloids Surf. A* **1994**, *1994*, 79−95.
(15) Tahani, A.; Vandamme, H.; Noik, C.; Levitz, P. *J. Colloid Interface Sci.* **1996**, *184*, 469−476.
(16) Somasundaran, P.; Turro, N. J.; Chandar, P. *Colloids Surf.* **1986**, *20*, 145−150.
(17) Huang, L.; Somasundaran, P. *Colloids Surf. A* **1996**, *117*, 235−244.
(18) Fan, A. X.; Somasundaran, P.; Turro, N. J. *Langmuir* **1997**, *13*, 506−510.
(19) Cummins, P. G.; Staples, E.; Penfold, J. *J. Phys. Chem.* **1990**, *94*, 3740−3745.
(20) Penfold, J.; Staples, E.; Tucker, I.; Cummins, P. *J. Phys. Chem.* **1996**, *100*, 18133−18137.
(21) Kline, S. R.; Kaler, E. W. *J. of Chem. Phys.* **1996**, *105*, 3813−3822.
(22) Kline, S. R.; Kaler, E. W. *Langmuir* **1996**, *12*, 2402−2407.
(23) Vanjara, A. K.; Dixit, S. G. *Adsorpt. Sci. Technol.* **1996**, *13*, 377−395.
(24) Söderlind, E.; Stilbs, P. *Langmuir* **1993**, *9*, 1678−1683.
(25) Söderlind, E.; Bjorling, M.; Stilbs, P. *Langmuir* **1994**, *10*, 890−898.
(26) Söderlind, E.; Stilbs, P. *J. Colloid Interface Sci.* **1991**, *143*, 586−588.
(27) Söderlind, E.; Stilbs, P. *Langmuir* **1993**, *9*, 2024−2034.
(28) Schonhoff, M.; Soderman, O. *J. Phys. Chem. B* **1997**, *101*, 8237−8242.
(29) Piedra, G.; Fitzgerald, J. J.; Ridenour, C. F.; Maciel, G. E. *Langmuir* **1996**, *12*, 1958−1966.
(30) Lee, E. M.; Thomas, R. K.; Cummins, P. G.; Staples, E. J.; Penfold, J.; Rennie, A. R. *Chem. Phys. Lett.* **1989**, *162*, 196−202.
(31) McDermott, D. C.; Lu, J. R.; Lee, E. M.; Thomas, R. K.; Rennie, A. R. *Langmuir* **1992**, *8*, 1204−1210.
(32) McDermott, D. C.; Kanelleas, D.; Thomas, R. K.; Rennie, A. R.; Satija, S. K.; Majkrzak, C. F. *Langmuir* **1993**, *9*, 2404−2407.
(33) McDermott, D. C.; McCarney, J.; Thomas, R. K.; Rennie, A. R. *J. Colloid Interface Sci.* **1994**, *162*, 304−310.
(34) Penfold, J.; Staples, E. J.; Tucker, I.; Thompson, L. J. *Langmuir* **1997**, *13*, 6638−6643.
(35) Rennie, A. R.; Lee, E. M.; Simister, E. A.; Thomas, R. K. *Langmuir* **1990**, *6*, 1031−1034.
(36) Lee, E. M.; Thomas, R. K.; Rennie, A. R. *Prog Colloid Polym. Sci.* **1990**, *81*, 203−208.
(37) Manne, S.; Cleveland, J. P.; Gaub, H. E.; Stucky, G. D.; Hansma, P. K. *Langmuir* **1994**, *10*, 4409−4413.
(38) Manne, S.; Gaub, H. E. *Science* **1995**, *270*, 1480−1482.
(39) Manne, S.; Schäffer, T. E.; Huo, Q.; Hansma, P. K.; Morse, D. E.; Stucky, G. D.; Aksay, I. A. *Langmuir* **1997**, *13*, 6382−6387.
(40) Grant, L. M.; Ducker, W. A. *J. Phys. Chem. B* **1997**, *101*, 5337−5345.
(41) Patrick, H. N.; Warr, G. G.; Manne, S.; Aksay, I. A. *Langmuir* **1999**, *15*, 1685−1692.
(42) Sivia, D. S.; Hamilton, W. A.; Smith, G. S. *Physica* **1991**, *173*, 121−138.
(43) Zhou, X. L.; Chen, S. H. *Phys. Rep.* **1995**, *257*, 223−348.
(44) Chen, S. H.; Zhou, X. L.; Carvalho, B. L. *Prog. Colloid Polym. Sci.* **1993**, *93*, 85−91.
(45) Hayter, J. B.; Zulauf, M. *Colloid Polym. Sci.* **1982**, *260*, 1023−1028.
(46) Lum Wan, J. A.; Warr, G. G.; White, L. R.; Grieser, F *Colloid Polym. Sci.* **1987**, *265*, 528−534.
(47) Butler, P. D.; Hamilton, W. A.; Magid, L. J.; Hayter, J. B.; Slawecki, T. M.; Hammouda, B. *Faraday Discuss.* **1996**, *104*, 65−78, General Discussion 88−91.
(48) Hamilton, W. A.; Butler, P. D.; Hayter, J. B.; Magid, L. J.; Kreke, P. J. *Physica B* **1996**, *221*, 309−319.
(49) Scattering length density was calculated for decane using data from Caponetti, E.; Causi, S.; De Lisi, R.; Floriano, M. A.; Milioto, S.; Triolo, R. *J. Phys. Chem.* **1992**, *96*, 4950−60.
(50) Lekner, J. *Theory of Reflection of Electromagnetic and Particle Waves*; Martinus Nijhoff: Dordrecht, 1987; Vol. Appendix A-5.
(51) Lekner, J. *Physica B* **1991**, *173*, 99−111.
(52) Russell, T. P. *Mater. Sci. Rep.* **1990**, *5*, 171−270.
(53) Lu, J. R.; Thomas, R. K. *J. Chem. Soc., Faraday Trans.* **1998**, *94*, 995−1018.
(54) Schulz, J. C. ReflectJCS, 1.00 ed.; University of Sydney: Sydney, 1997.
(55) It may be proved as a general result that monotonic (step) profiles reflect less than the clean interface (see, for instance, section 5-4 of ref 50).
(56) Fragneto, G.; Thomas, R. K.; Rennie, A. R.; Penfold, J. *Langmuir* **1996**, *12*, 6036−6043.
(57) Favoriti, P.; Monticone, V.; Treiner, C. *J. Colloid Interface Sci.* **1996**, *179*, 173−180.
(58) Monticone, V.; Treiner, C. *J. Colloid Interface Sci.* **1994**, *166*, 394−403.
(59) Desbene, P. L.; Portet, F.; Treiner, C. *J. Colloid Interface Sci.* **1997**, *190*, 350−356.
(60) Portet, F.; Desbene, P. L.; Treiner, C. *J. Colloid Interface Sci.* **1997**, *194*, 379−391.
(61) Portet, F.; Desbene, P. L.; Treiner, C. *J. Colloid Interface Sci.* **1996**, *184*, 216−226.
(62) Gruen, D. W. R. *J. Phys. Chem.* **1985**, *89*, 153−163.
(63) Gruen, D. W. R. *J. Phys. Chem.* **1985**, *89*, 149−153.
(64) Gruen, D. W. R. *J. Colloid Interface Sci.* **1981**, *84*, 281−283.